Applied Catalysis B: Environmental 189 (2016) 99–109

Contents lists available at ScienceDirect

Applied Catalysis B: Environmental

journal homepage: www.elsevier.com/locate/apcatb

TiO2 modified with polyoxotungstates should induce visible-light absorption and high photocatalytic activity through the formation of surface complexes

Julián A. Rengifo-Herrera[a,*], Mirta Blanco[a], Julien Wist[b], Pierre Florian[c], Luis R. Pizzio[a,*]

[a] Centro de Investigación y Desarrollo en Ciencias Aplicadas "Dr. J.J. Ronco" (CINDECA), Departamento de Química, Facultad de Ciencias Exactas, UNLP-CCT La Plata, CONICET, 47 No. 257, 1900 La Plata, Buenos Aires, Argentina
[b] Departamento de Química, Universidad del Valle, A. A. 25360, Cali, Colombia
[c] CNRS, CEMHTI UPR3079, Université d'Orléans, F-45071 Orléans, France

ARTICLE INFO

Article history:
Received 22 October 2015
Received in revised form 10 February 2016
Accepted 12 February 2016
Available online 18 February 2016

Keywords:
Tungstophosphoric acid
Tungstosilicic acid
TiO_2 with visible light absorption
Heterogeneous photocatalysis
Heteropolyacids

ABSTRACT

TiO_2 nanospherical particles prepared by the sol-gel method were modified with tungstophosphoric (TPA) and tungstosilicic acid (TSA) at 30% (w/w) and then annealed at 500 °C for 2 h. Materials were characterized by multitechniques, such as scanning electron microscopy with energy dispersive X-ray spectroscopy (SEM-EDX), FT-Raman spectroscopy, X-ray photoelectron spectroscopy (XPS), X-ray diffraction (XRD), diffuse reflectance spectroscopy (DRS), ^{31}P, ^{1}H and ^{29}Si magic angle spinning nuclear magnetic resonance (MAS-NMR). Acidity and isoelectric point measurements were also performed. DRS results showed evidence of visible light absorption of TiO_2-TPA and TiO_2-TSA. MAS-NMR, XPS and FT-Raman characterization revealed evidence of a strong interaction between the Keggin anion of TPA or TSA and TiO_2 surfaces, possibly promoted by the formation of surface heteropolyacid-TiO_2 complexes; the latter should be responsible of its visible light absorption. Photocatalytic activity was evaluated in the degradation of malachite green (MG), a cationic triphenylmethane dye, and 4-chlorophenol (4-CP) aqueous solutions under UV-A and visible light irradiations. Under UV-A light, TPA-TiO_2 and TSA-TiO_2 materials showed high photocatalytic activity towards MG degradation, even higher than that of TiO_2 P-25. When 4-CP was degraded, TiO_2 P-25 exhibited higher photocatalytic activity. Under visible light irradiation and using the modified photocatalysts, malachite green oxidation was achieved, while 4-chlorophenol reached almost 20% of degradation. Mechanisms of photocatalytic oxidation either under UV-A or visible irradiation are discussed.

1. Introduction

During two decades, the potential of heterogeneous photocatalysis over TiO_2 to destroy a wide range of waterborne pollutants and microorganisms has aroused enormous interest [1,2]. These studies have positioned this technology as a promising process for the detoxification and disinfection of wastewaters.

However, nowadays several limitations have been highlighted and must be overcome for the successful application of heterogeneous photocatalysis over TiO_2 for water detoxification under solar light conditions. Among them, the absorption of visible light represents an enormous limitation in solar-driven photocatalytic processes since it is well known that TiO_2, in any of its crystalline structures, anatase or rutile, absorbs only UV light, which is not abundant on the planetís surface (4–7% of total sunlight hitting the earth surface) [3,4]. Moreover, the high electron-hole recombination rate is an important issue since most of the charge carriers induced on TiO_2 by UV-light absorption undergoes fast recombination [5].

For this reason, many efforts have been focused on preparing TiO_2 based materials that absorb visible light while hindering electron-hole recombination [6–10]. The addition of heteropolyoxometallates (POMs), which are clusters of transition metals and oxygen, to TiO_2 has risen as a successful alternative to synthesize visible light absorbing materials with high photocatalytic activity, especially because the electronic features of POMs could decrease the electron-hole recombination [11–13].

The mechanism by which TiO_2 modified by POMs absorbs visible light is not yet a clear issue and many mechanisms have been

* Corresponding authors at: CINDECA, Calle 47 No. 257, 1900 La Plata, Argentina.
E-mail addresses: julianregifo@quimica.unlp.edu.ar (J.A. Rengifo-Herrera), lrpizzio@quimica.unlp.edu.ar (L.R. Pizzio).

http://dx.doi.org/10.1016/j.apcatb.2016.02.033
0926-3373/

proposed in the literature. For instance, Yu et al. [14] have suggested that visible light absorption of TiO_2 samples modified with tungstophosphoric acid (TPA) and annealed at 350 °C is due to the presence of phosphorus doping (P-doping) and WO_3, both species arising from the thermal degradation of TPA. However, this point is not clear since some studies reported in the literature have demonstrated that the Keggin anion of TPA is stable at temperatures up to 400 °C, even in TiO_2 samples modified with this POM [15].

On the other hand, Li et al. [16] and Lu et al. [17] have suggested that visible light absorption of the TPA/TiO_2 materials annealed at high temperatures is due to the charge transfer from O 2p orbitals of the valence band to the new conduction band formed by the hybridization of Ti 3d from TiO_2 and W 5d orbitals from the Keggin anion (band gap narrowing). In this case, evidence is given about the TPA Keggin anion remaining unaltered on the TiO_2 surface and about the formation of Ti-O-W bonds between terminal W = O groups from the Keggin unit and surface Ti atoms. However, the band gap narrowing caused by orbital hybridization is a controversial issue in visible light absorbing TiO_2 materials. Regarding N-doped TiO_2, Serpone [18] argues that hybridization of N 2p with O 2p orbitals should not be possible and might require high dopant loadings, altering the original integrity of the metal oxide.

Recently, our research group has prepared TiO_2 materials modified by tungstophosphoric acid (TPA) and tungstosilicic acid (TSA) via sol-gel synthesis at high temperatures (>400 °C) that exhibited high photocatalytic activity [19–21]. These studies found evidence about increasing the load of POMs in the TiO_2 samples, materials exhibited high visible light absorption and high pohotocatalytic activity, being the materials containing 30% (w/w) of TPA or TSA and annealed at 500 °C, those with the highest visible light absorption and photocatalytic activity [19–21]. In 2011, we claimed that visible light absorption of TPA-TiO_2 materials could be due to the formation of visible light absorbing WO_x species, such as WO_3 coming from the partial thermal degradation of TPA, although there is evidence that the Keggin anion remains unaltered on TiO_2 [19]. In 2014, we prepared several TPA-TiO_2 materials by impregnation of TPA at different pH values (1.0, 2.0, 5.0 and 10.0) [21]. Visible light absorption was only observed in the samples impregnated at low pH (1.0 and 2.0). At these pH values, the Keggin anion is the main TPA species in solution, leading us to suggest that the cause for visible light absorption in the TPA-TiO_2 systems could be attributed to the strong interaction between the Keggin anion and TiO_2 surface yielding a TPA-TiO_2 surface complex rather than to the presence of WO_x species.

Regarding the photocatalytic activity of TiO_2 materials modified by heteropolyoxometallates, mainly by TPA, a common conclusion can be drawn: these materials show high photocatalytic activity either under UV or visible light irradiation [11–22]. Indeed, few studies suggesting mechanisms of photocatalytic activity have been reported. Under UV light irradiation, it is clear that photocatalytic activity is caused by the low electron-hole recombination in TPA-TiO_2 materials since the electronic transfer of photoinduced conduction band electrons to TPA species could be thermodynamically favored [11–13]. However, the mechanisms under visible light irradiation are yet under debate. For instance, Yu et al. [14] suggested that P-doping in TiO_2 should be responsible for visible light absorption, thus yielding photoinduced electrons and holes. The valence band holes on TiO_2 should be responsible for the oxidation of organic compounds, while the conduction band electrons should be transferred to WO_3 (since the conduction band of P-doped TiO_2 is more cathodic than the conduction band of WO_3). Yang et al. [22] proposed a mechanism for the degradation of methylene blue under visible light irradiation by TPA-TiO_2 materials. They claimed that TPA-TiO_2 nanocomposites absorb visible light generating electron-hole pairs on TiO_2 particles and then, the conduction band electrons are transferred to TPA decreasing the electron-hole recombination. Moreover, the high photocatalytic activity of such materials is also attributed to their bimodal porous structure, which provides enhanced mass transport and high adsorption of methylene blue on the photocatalyst surface. It is not clear, however, how these materials can absorb visible light. On the other hand, Lu et al. [17] have suggested that the oxidation of Rhodamine B aqueous solutions by TPA-TiO_2 composites is due to the generation of electron-hole pairs by visible light irradiation. This excitation is possible since TPA might cause a band gap narrowing on TiO_2, thus photoinduced valence band holes or $^{\bullet}OH$ radicals should be responsible for Rhodamine B oxidation.

In our study published in 2011 [19] we reported that TPA-TiO_2 materials showed a high activity towards the oxidation of malachite green (MG), a cationic triphenylmethane dye, under UV and visible light irradiation. We concluded that visible light activity could be attributed to the excitation of WO_x species producing oxidative forms responsible for malachite green abatement. Regarding the photocatalytic activity of materials containing tungstosilicic acid (TSA) with either UV or visible light irradiation, there are not many studies in the literature. For instance, the preparation of monovacant Keggin anion-silica composites (SiW_{11}-SiO_2) leads to the formation of materials with an interesting photocatalytic activity towards malic acid oxidation upon UV light irradiation. The authors suggested that this activity was related to the excitation of the Keggin anion of the polyoxometallates by UV irradiation [23,24]. Recently, we reported that TSA-TiO_2 materials synthesized via the sol-gel process exhibit visible light absorption and high photocatalytic activity during 4-chlorophenol (4-CP) oxidation upon UV + visible light irradiation [20].

The main aim and novelty of this study was to gain a better understanding, by performing a multitechniques characterization and evaluating the photocatalytic activity upon UV-A and visible light, about why TiO_2 nanoparticles modified with polyoxometallates absorb visible light and which should be their photocatalytic mechanisms to the organics abatement upon different light sources irradiation.

2. Experimental

2.1. Materials

The chemical substances used to synthesize the TiO_2-based samples and perform the photocatalytic tests were: titanium tetraisopropoxide (99%, Sigma-Aldrich), urea (99%, Sigma-Aldrich), tungstophosphoric acid ($H_3PW_{12}O_{40}{\cdot}23H_2O$), tungstosilicic acid ($H_4SiW_{12}O_{40}{\cdot}23H_2O$) (99%, Fluka), malachite green oxalate (MG) (99%, Sigma-Aldrich), 4-chlorophenol (4-CP) (99%, Fluka), ethanol (Merck, absolute grade), HCl (37%, Carlo Erba). All chemicals were used as received.

2.2. Sample preparation

Titanium isopropoxide (26.7 g) was mixed with absolute ethanol (186.6 g) and stirred for 10 min under N_2 at room temperature to obtain a homogeneous solution, then 0.33 mL of 0.28 M HCl aqueous solution was dropped slowly into the above mixture to catalyze the sol-gel reaction and was left to stand for 3 h. Then, 120 g of urea-alcohol-water (1:5:1 wt ratio) solution was added to the hydrolyzed solution under vigorous stirring, to act as template, together with an ethanol solution of $H_3PW_{12}O_{40}{\cdot}23H_2O$ (TPA) or $H_4SiW_{12}O_{40}{\cdot}23H_2O$ (TSA). The amount of TPA or TSA solutions was fixed in order to obtain a concentration of 30% TPA or TSA (W concentration of 22.9% TPA (w/w) and 23.5% TSA (w/w)) by weight in the final material.

The gels were dried at room temperature in a beaker. The solids were ground into powder and extracted with distilled water for three periods of 24 h to remove urea, in a system with continuous stirring. Finally, the solids were thermally treated at 500 °C for 2 h. The samples will be named TPA-TiO_2 and TSA-TiO_2, respectively.

2.3. Sample characterization

2.3.1. Diffuse reflectance spectroscopy (DRS)

The diffuse reflectance spectra of the materials were recorded using a UV-vis Lambda 35, PerkinElmer spectrophotometer, to which a diffuse reflectance chamber Labsphere RSA-PE-20 with an integrating sphere of 50 mm diameter and internal Spectralon coating is attached, in the 250–800 nm wavelength range. Spectralon was used as reference.

2.3.2. X-ray diffraction (XRD) measurements

X-ray diffraction patterns of the samples were recorded using Philips PW 1732 equipment with a built-in recorder and CuKα radiation, nickel filter, 20 mA and 40 kV in the high voltage source, and scanning angle between 5 and 60°of 2θ at a scanning rate of 1° per min.

2.3.3. Nuclear magnetic resonance spectroscopy (NMR)

^{29}Si and ^{31}PMAS NMR experiments were performed on a 9.4 T Avance Bruker Spectrometer operating at 161.9 MHz and 79.5 MHz, respectively. We used a 4 mm diameter rotor spinning at 10 kHz and applied Bloch decay (single pulse acquisition) with a radio-frequency field of 100 kHz (^{31}P) and 35 kHz (^{29}Si) and pulse width of 10°. Due to the very small amount of NMR active nuclei in the sample, no relaxation time measurement could be performed and we chose a recycle delay of 15 s (^{31}P) and 1 s (^{29}Si) based on various trials while accumulating between 21120 (3.7 days) and 642600 (7.5 days) scans, respectively. ^{1}H MAS-NMR experiments were performed on a 17.6 T Avance III Bruker spectrometer operating at 750.3 MHz. Hahn echo experiments were performed spinning at 30 kHz to remove the large probe background using a delay of 5 rotor periods (160 μs) and a radio-frequency field strength of 100 kHz ^{31}P spectra are referenced to a 1 M solution of H_3PO_4, whereas ^{29}Si and ^{1}H ones are referenced to tetramethylsilane.

2.3.4. X-ray photoelectron spectroscopy (XPS)

XPS analyses were carried out with XPS Analyzer Kratos model Axis Ultra with a monochromatic AlKα and charge neutralizer. The deconvolution software program was provided by Kratos, the manufacturer of the XPS instrument. All the binding energies were referred to the C1s peak at 285 eV of adventitious carbon. Powder samples were prepared by deposition of the solid on carbon type stuck to the sample holder.

2.3.5. Fourier transform Raman spectroscopy (FT-Raman)

Raman scattering spectra were recorded on a Raman Horiba Jobin-Yvon T 64000 instrument with an Ar+ laser source of 488 nm wavelength in a macroscopic configuration.

2.3.6. Acidity measurements by potentiometric titration

The solid (0.05 g) was suspended in acetonitrile (Merck) and stirred for 3 h. Then, the suspension was titrated with 0.05 N *n*-butylamine (Carlo Erba) in acetonitrile using Metrohm 794 Basic Titrino apparatus with a double junction electrode.

2.3.7. Isoelectric point (IP)

The isoelectric point was calculated from zeta potential measurements at different pH values. Laser Doppler velocimetry was applied to characterize the electrophoretic mobility (EPM) of the particles using a Malvern Zetasizer Nano ZS. Measured EPMs were converted to zeta potential using the Smoluchowski equation:

$$U = \varepsilon \frac{\zeta}{\mu} \quad (1)$$

where U is the electrophoretic mobility, ε is the dielectric constant of the solution, μ is its viscosity, and ζ is the zeta potential.

Disposable folded capillary cells were employed. First, 0.05 g of solid was suspended in 15 mL of Milli-Q water and the solution pH was modified by adding HCl or NaOH.

2.3.8. Scanning electron microscopy with energy dispersive X-ray spectroscopy (SEM-EDX)

The secondary electron micrographs of the samples were obtained by scanning electron microscopy (SEM) using Philips 505 Model equipment and EDAX 9100 analyzer at a working potential of 15 kV and graphite-supported samples metallized with gold.

2.3.9. Atomic absorption spectrometry (AAS)

Tungsten (W) determination was carried out using an atomic absorption spectrometer Varian AA model 240 spectrophotometer. The calibration method was used with in-house prepared standards. Analyses were carried out at a wavelength of 254.9 nm, bandwidth 0.3 nm, lamp current 15 mA, phototube amplification 800 V, burner height 4 mm, and acetylene-nitrous oxide flame (11:4 volumetric ratio).

2.4. Photocatalytic activity

TiO_2 (1.0 gl^{-1}) was added to a 1.0×10^{-5} M aqueous malachite green oxalate solution or 1.0×10^{-4} M aqueous solution of 4-chlorophenol contained in 50 mL cylindrical Pyrex bottles. Prior to UV or blue-light irradiation, the resulting suspension was kept under magnetic stirring in the dark for ca. 30 min to ensure that dye/TiO_2 or 4-chlorophenol/TiO_2 surface adsorption/desorption processes were reached. The suspension was then irradiated by 5 UV black light lamps Philips TLD 18W (emission spectra: 330–400 nm and UV intensity between 300 and 400 nm: 38 W m^{-2}) or 5 blue fluorescent lamps Philips TLD-18W (emission spectra: 400–500 nm with UV intensity: 0.1 W m^{-2} and global intensity between 290 and 1100 nm: 60 W m^{-2}). UV and global intensity were monitored with a Kipp & Zonen (CM3) power meter (Omni instruments Ltd, Dundee, UK). The samples taken at different illumination times were filtered through membranes of 0.22 μm pore size, and the discoloration of the MG solution was followed by UV-vis spectrophotometry (Varian Cary 1-E) monitoring the absorbance at 618 nm. The initial pH of each solution was adjusted to 5.0 by adding HCl (Cl^- concentration was kept below 1 mM). The running temperature was never higher than 38 °C.

The W leaching experiments were performed by adding amounts of TPA-TiO_2 or TSA-TiO_2 materials to 50 mL of distilled water until a solid concentration of 1 g l^{-1} was obtained. These suspensions were then irradiated for 4 h with UV-A light. Finally, the solutions were centrifuged and the supernatant was analyzed by AAS.

3. Results

3.1. TiO_2, TPA-TiO_2 and TSA-TiO_2 characterization

Fig. 1 shows the DRS spectra of pristine TiO_2 and TiO_2 modified with TPA or TSA. TPA-TiO_2 and TSA-TiO_2 samples exhibit a broad absorption band in the UV region due to the presence of TiO_2, as well as TPA or TSA. TiO_2 shows light absorption at wavelengths below 400 nm mainly due to electronic promotion from the O 1s valence band to the Ti 2p conduction band [25]. On the other hand,

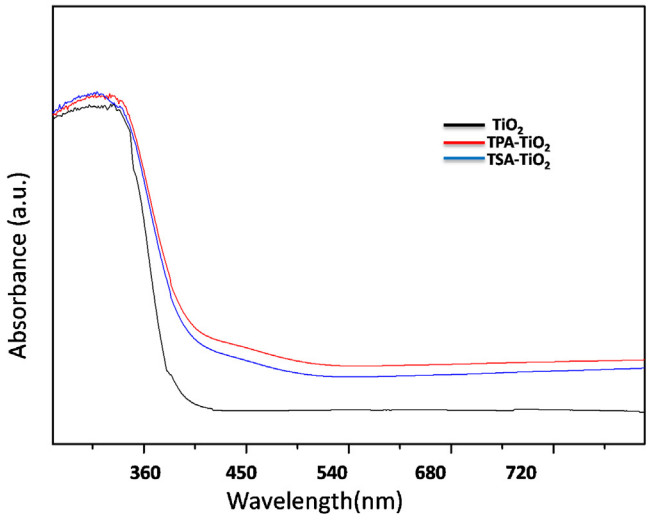

Fig. 1. DRS spectra of TiO_2 (black line), TPA-TiO_2 (red line) and TSA-TiO_2 (blue line) samples. (For interpretation of the references to colour in this figure legend, the reader is referred to the web version of this article.)

TPA and TSA exhibit two intense bands in the range 200–450 nm [26], attributed to the charge transfer from bridging or terminal O 2p to W 5d (W-O-W and W-Od).

However, it was not possible to identify single absorption bands corresponding to TPA and TSA in the TPA-TiO_2 and TSA-TiO_2 samples, respectively. In addition, DRS results revealed that TPA-TiO_2 and TSA-TiO_2 samples absorb visible light at wavelengths up to 400 nm.

The W content in the TPA-TiO_2 and TSA-TiO_2 samples was estimated as the difference between the W amount contained in the TPA or TSA solutions and the remaining amount of W in the solutions obtained during the washing of xerogels. The amount of W was determined by atomic absorption spectrometry. The results obtained revealed that the W content in the samples was 22.6% (w/w) and 23.2% (w/w) for the TPA-TiO_2 and TSA-TiO_2 samples, respectively, which agrees well with the initial W amount added as TPA and TSA during the synthesis (W concentration 22.9% TPA (w/w) and 23.5% TSA (w/w)).

The SEM images (S1) showed that all the synthesized samples are composed of spherical nanoparticles with an average diameter of around 500 nm. This morphology is produced by the presence of urea during sample preparation. As already reported [19,27], urea decomposition in aqueous solution during sol-gel synthesis might smoothly increase the pH, leading to the formation of TiO_2 nanoparticles with a controlled morphology, in this case, spherical. On the other hand, the EDX measurements revealed the existence of W signals Lα1 and Mα1 at 8.396 and 1.779 KeV, respectively in TiO_2-TPA samples, while TiO_2-TSA samples showed the same W signals and a new one at 1.838 KeV assigned to Si Mα line. This fact is closely related to the presence of POMs or some of their degradation by-products on the modified TiO_2 surface.

The XRD patterns of the synthesized samples are shown in S3. All the samples exhibited peaks related to the anatase phase of TiO_2 ($2\theta = 25.3^\circ$, 37.9°, 47.8° and 54.3°) [28]. TPA and TSA peaks were not found, probably because heteropolyacids (HPAs) are highly dispersed on the titania matrix or as a noncrystalline phase. Fig. 3 also shows the line broadening that took place, which is an indication of a low crystallinity. Indeed, previous studies indicated that the presence of TPA or TSA produces a detrimental effect on the crystallinity of TiO_2 [15,29].

The FT-Raman scattering spectra (Fig. 2A) revealed the presence of the typical peaks often linked to the presence of anatase TiO_2 in all the TiO_2 samples. Anatase TiO_2 belongs to the tetragonal space group $D_{4h}{}^{1g}$ ($I4_1/amd$), which exhibits six Raman active modes ($A_{1g} + 2B_{1g} + 3E_g$) at 141.3 cm^{-1} (E_g), 197 cm^{-1} (E_g), 394.4 cm^{-1} (B_{1g}), 516.1 cm^{-1} (A_{1g}, B_{1g}), and 636.7 cm^{-1} (E_g) [30]. On the other hand, the FT-Raman spectrum of bulk TPA showed Raman vibration bands typically assigned to the Keggin anion at 1080, 990, 930, and 890 cm^{-1}, which are attributed to antisymmetric vibrations of P-O, W = O and W-O-W bonds [31]. TSA exhibited FT-Raman peaks at 1000 cm^{-1}, 976 cm^{-1} and 926 cm^{-1} corresponding to ν_s (W-O), $_{as}$ (W-O) and ν_{as} (W-O-W), respectively, which agree very well with those of the Keggin anion of TSA [32,33].

Fig. 2C shows that Raman peaks of TPA and TSA between 1000 and 800 cm^{-1} undergo an important broadening when HPAs are present on TiO_2. Furthermore, the main Raman scattering peak of TiO_2 at 141 cm^{-1} exhibited a strong blue shift and broadening (Fig. 2B). Some authors have attributed the shift and broadening of the Raman band at 141 cm^{-1} in anatase TiO_2 to deviations from stoichiometry [34,35]. This Raman band arises from O-Ti-O band-bending-type vibrations; thus this shift may be related to the presence of oxygen deficiencies or disorders induced by minority phases [30,34–36]. Moreover, Li et al. [16] have argued that the shift and broadening of the Raman vibration modes of TPA and TiO_2 could also be associated with a strong interaction between the TiO_2 network and TPA.

The XPS spectra are shown in Fig. 3. The literature reports a doublet for the W 4f XPS peak of pure TPA and TSA with binding energies (BE) at 37.9 and 35.8 eV corresponding to W (VI) typically present in the Keggin anions of TSA and TPA [37,38]. On the other hand, high resolution XPS spectra of W 4f from TiO_2-TPA and TiO_2-TSA samples (Fig. 3a and b) also exhibited a doublet with BE at 38.2 and 36.2 eV, indicating that these peaks underwent a slight shift, which is too small for a change in the oxidation state of W atoms, and should be related to some interaction between the Keggin anion and the TiO_2 surface.

Figs. 3c and d show the high resolution XPS spectra for Ti 2p and O 1s signals. Often, TiO_2 shows a Ti 2p doublet signal with BE at 459 and 465 eV due to the presence of Ti (IV), while the O 1s signal reveals two peaks with BE at 530.6 and 532.2 eV due to Ti-O and Ti-OH bonds, respectively [39,40]. The TiO_2-TPA and TiO_2-TSA samples did not show any change of the XPS Ti 2p signal; however, the O 1s peak at 530 eV underwent a slight shift.

The acidity measurements of the catalysts by means of potentiometric titration with *n*-butylamine led us to estimate the acid strength and the number of acid sites and their distribution. As a

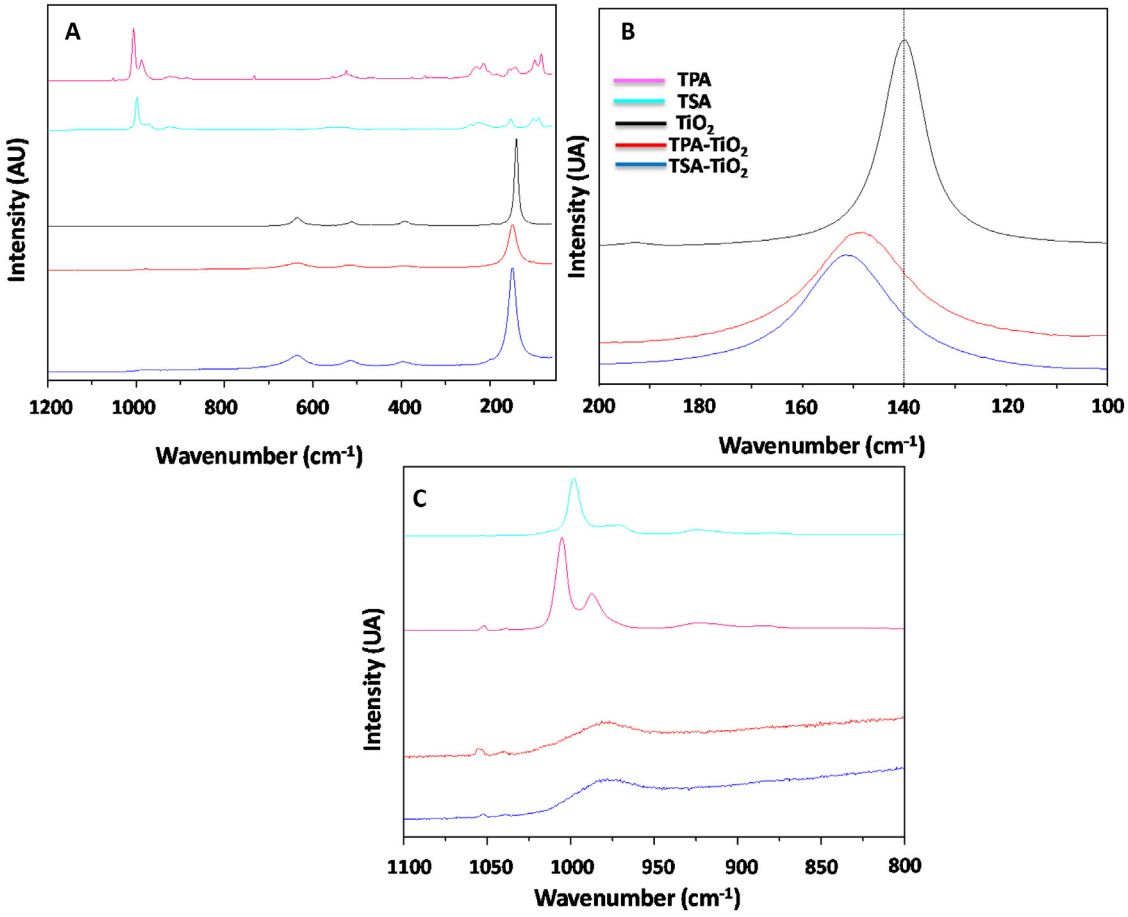

Fig. 2. FT-Raman spectra of TPA, TSA, TiO_2, TPA-TiO_2 and TSA-TiO_2 samples.

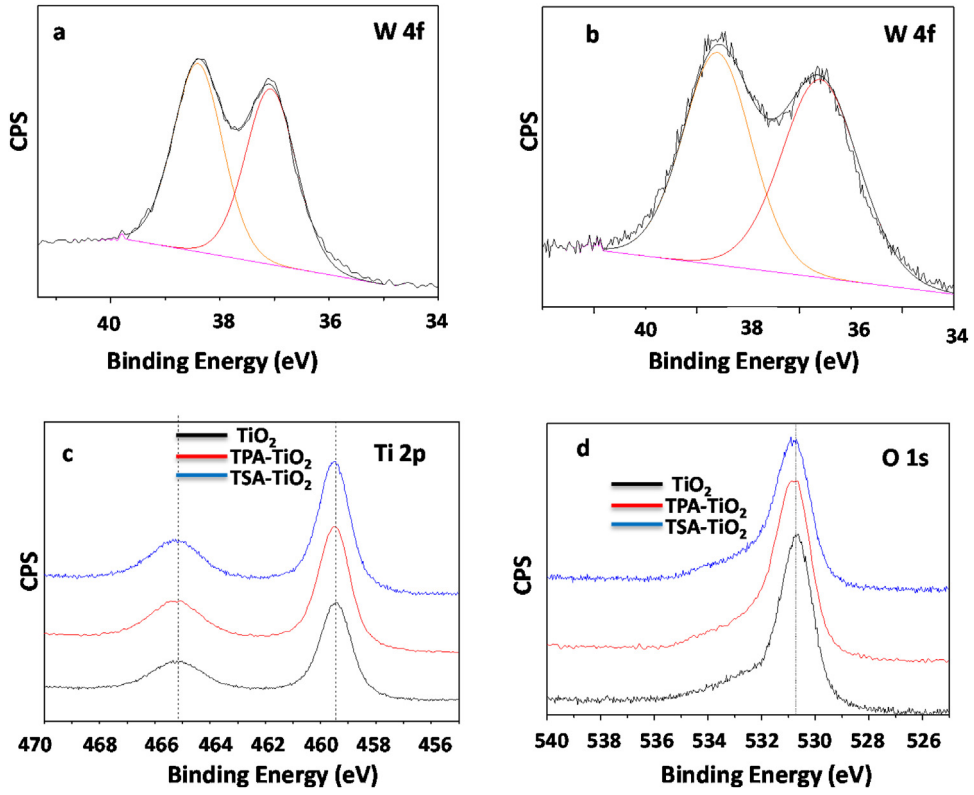

Fig. 3. XPS spectra of W 4f signal in (a) TPA-TiO_2, (b) TSA-TiO_2 samples. (c) Ti 2p and (d) O 1s signals in TiO_2, TPA-TiO_2 and TSA-TiO_2 samples.

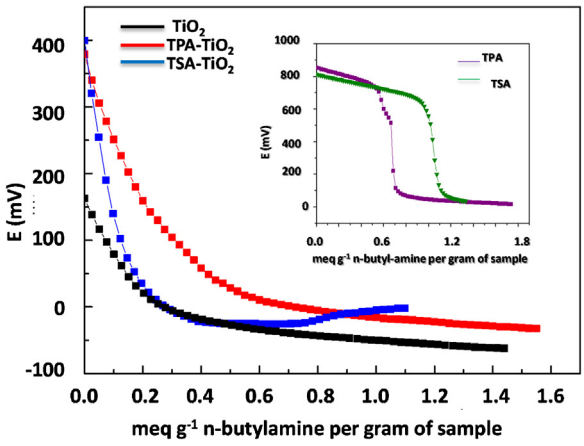

Fig. 4. Potentiometric titration with *n*-butylamine of TiO_2, TPA-TiO_2 and TSA-TiO_2 samples (TPA and TSA as inset).

criterion to interpret the obtained results, it was suggested that the initial electrode potential (E_i) indicates the maximum acid strength of the sites and the value of meq amine g^{-1} solid where the plateau is reached indicates the total number of acid sites. The acid strength of these sites may be classified according to the following scale [41,42]:

$$E_i > 100\,mV(very strong sites),\ 0 < E_i < 100\,mV(strong sites),$$

$$-100 < E_i < 0(weak sites) and E_i < -100\,mV(very weak sites).$$

According to the potentiometric titration curves of TiO_2, TiO_2-TPA and TiO_2-TSA samples (Fig. 4), the acid strength of the TiO_2-TPA and TiO_2-TSA samples (E_i = 378 and 398 mV, respectively) is higher than that of TiO_2 (E_i = 150 mV) but lower than that of bulk TPA and TSA (E_i = 800 and 850 mV, respectively). The titration curves of bulk TPA and bulk TSA are shown in the inset of Fig. 4. Bulk TPA and TSA showed a very high acidity (E_i = 800 and 850 mV, respectively). The lower acid strength of the TiO_2-TPA and TiO_2-TSA samples compared to bulk HPA could be assigned to the fact that the protons in TPA and TSA are present as $H^+(H_2O)_n$ species, whereas in the titania-modified samples they are interacting with the Ti-OH groups.

The interaction can be assumed to be of the electrostatic type due to the transfer of protons to Ti-OH sites according to:

$$Ti\text{-}OH + H_3PW_{12}O_{40} \rightarrow (Ti\text{-}OH_2^+)(H_2PW_{12}O_{40}^-) \quad (2)$$

$$2Ti\text{-}OH + H_3PW_{12}O_{40} \rightarrow (TiOH_2^+)_2(HPW_{12}O_{40}^{2-}) \quad (3)$$

$$Ti\text{-}OH + H_4SiW_{12}O_{40} \rightarrow (TiOH_2^+)_x(H_{4-x}SiW_{12}O_{40}^{-x}) \quad (4)$$

The z-potential measurements were performed to determine the isoelectric point (IP) of the solids (Table 1). Synthesized pristine anatase TiO_2 exhibited an IP of 5.7, which agrees very well with the IP of anatase TiO_2 (IP 6.0) [43]. On the other hand, the samples containing heteropolyacids showed an important decrease of their IP. The TiO_2-TPA sample exhibited an IP close to 1.8, while the IP of the TiO_2-TSA sample was 3.5. The presence of acid sites evidenced by the acidity measurements could be closely linked to these observations.

Table 1
Isoelectric points of samples.

Sample	pH_{pzc}
TiO_2	5.7
TiO_2-TPA-30%	1.8
TiO_2-TSA-30%	3.5

The MAS-NMR measurements of ^{31}P, ^{29}Si and ^{1}H nuclei were also performed. Results of ^{31}P MAS-NMR of bulk TPA showed a doublet at −14.7 ppm and −15.0 ppm, which can very probably be related to the hydrated Keggin anion of tungstophosphoric acid ($H_3PW_{12}O_{40}{\cdot}6H_2O$) [44,45] (Fig. 5a.2). However, the spectrum of TPA-TiO_2 sample exhibited an intense signal at −13.5 ppm and also a broad peak ranging from 1 to −20 ppm (Fig. 5a.1). The deconvolution of the latter signal (Fig. 5a.3) revealed the presence of small peaks at −11.2 and a wide signal at −12 ppm, which was absent in the "blank" experiment performed on the pure TiO_2 precursor. The peak at −13.5 ppm could be related to the presence of the Keggin anion of TPA interacting with the TiO_2 surface by forming surface species such as $(\equiv TiOH_2^+)(H_2PW_{12}O_{40}^-)$ and $(\equiv TiOH_2^+)_2(HPW_{12}O_{40}^{2-})$ [29,46] or surface complex with the formation of Ti—O—W bonds between TPA and TiO_2. On the other hand, the wide signal at −12.0 and the small peak at −11.2 ppm should be due to the presence of dimeric and lacunar species [31] of TPA ($[P_2W_{21}O_{71}]^{6-}$ and $[PW_{11}O_{39}]^{7-}$, respectively), the former presenting a large distribution of phosphorus environments, as evidenced by its important ^{31}P line width. The ^{29}Si solid NMR data are shown in Fig. 5b. The ^{29}Si signal for bulk TSA (Fig. 5b.2) exhibited a narrow peak at −84.7 ppm, which corresponds to the Keggin anion [47]. In TSA-TiO_2 this signal showed a tiny shift (ca. 0.3 ppm) since a peak at −85 ppm was detected (Fig. 5b.1). Furthermore, a broad peak localized between −100 and −120 ppm and centered at ca. −110 ppm was also observed. This latter signal is consistent with the presence of amorphous silica Q_4 species or lacunar species such as $[SiW_{11}O_{39}]^{8-}$ coming from the partial degradation of TSA [33,47].

Moreover, ^{1}H MAS-NMR characterization was also done (Fig. 6a and b). The ^{1}H spectra of bulk TPA and TSA (which have not been previously dehydrated) showed two peaks at high and low fields (at 7.5 and 6.8 ppm for TPA and 7.8 and 6.9 ppm for TSA), which could be related to interactions of water with protons of Keggin anions by forming H_3O^+ [45] (Fig. 6(a.3) and (b.3)).

Pristine TiO_2 samples exhibited two signals, a first intense and broad peak with a chemical displacement at ca. 5.6 ppm, probably due to bridging titanol groups (Ti-OH) and a second small and broad peak at 1.5 ppm, which could correspond to terminal titanol groups on the TiO_2 surface [48] (Fig. 6(a.2) and (b.2)).

The TPA-TiO_2 and TSA-TiO_2 samples (Fig. 6a.1 and b.1) showed the intense and broad signal at 5.5 ppm assigned to bridging titanol groups [48]. This peak is broader in samples containing TPA and TSA than in pristine TiO_2. The TSA-TiO_2 sample revealed two new signals at ca. 3.5 and 1.1 ppm, which could be related to the presence of silanol groups, such as those in SiO_2 [48]. A very small peak can also be observed on the left tail of the main component at 6.8 ppm, i.e., very close to the position of the ^{1}H peak of bulk TSA.

Fig. 7 shows the spectra of the same samples with a long (5 ms) echo delay that removes all fast relaxing components, such as the strongly dipolar-coupled titanol groups, while keeping the isolated or rapidly moving species. The above-mentioned tiny signal is then observed in both TPA-TiO_2 and TSA-TiO_2 samples at 6.8 ppm, in agreement with the presence of Keggin anions of TPA and TSA interacting with the TiO_2 surface and hence confirming the presence of acid sites on the surface. It is also interesting to note that the appearance of those surface species in the same long delay echo acquisition means that they are very probably mobile, at least on the NMR time scale. The remaining broad peak observed for TiO_2-TPA could probably be related to the broad peak observed in the ^{31}P spectra, i.e., decomposed TPA.

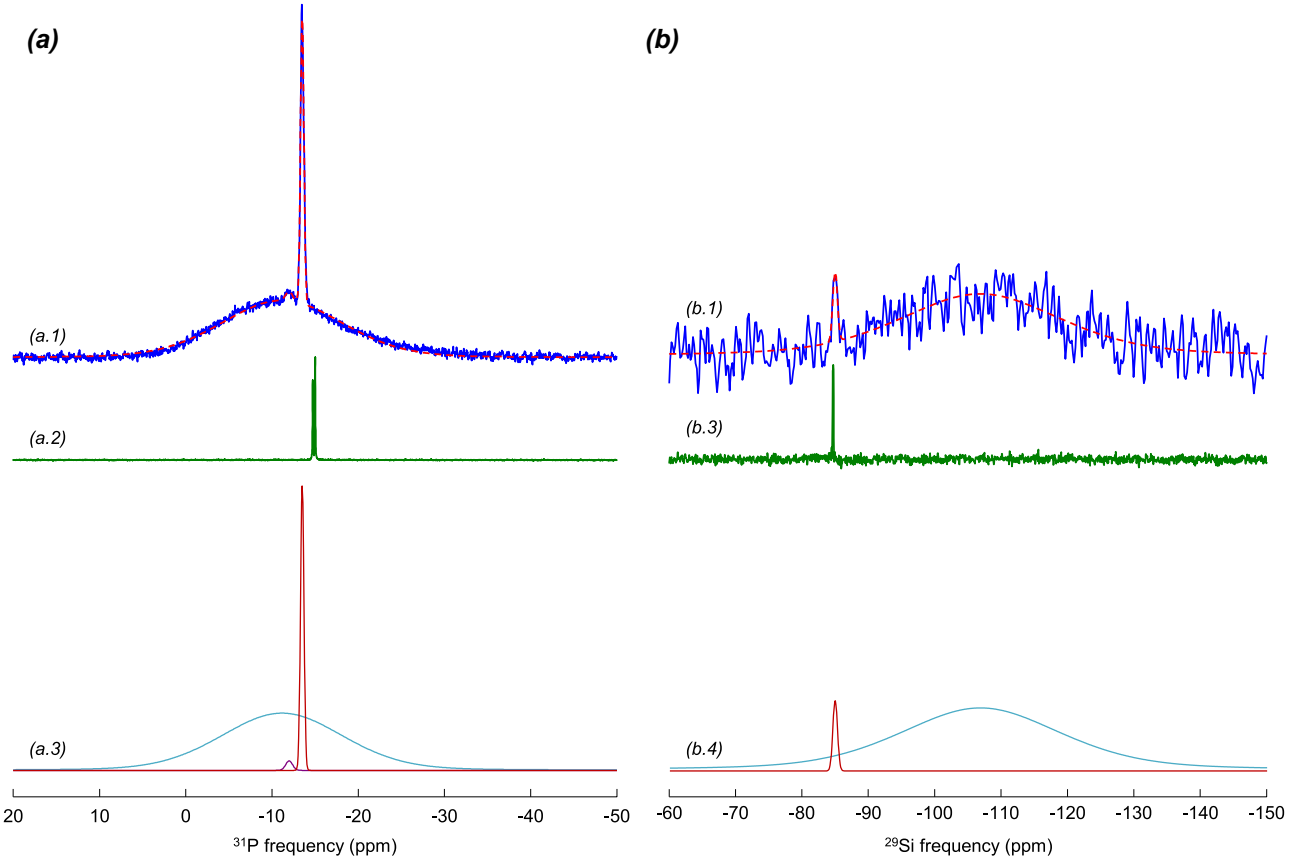

Fig. 5. (a) ^{31}P MAS-NMR spectra of (a.1) TPA-TiO_2 and (a.2) bulk TPA samples (a.3) the three individual components of the simulation are displayed. (b) ^{29}Si MAS-NMR spectra of (b.1) TSA-TiO_2 and (b.2) bulk TSA (b.3), the two individual components of the simulation are displayed.

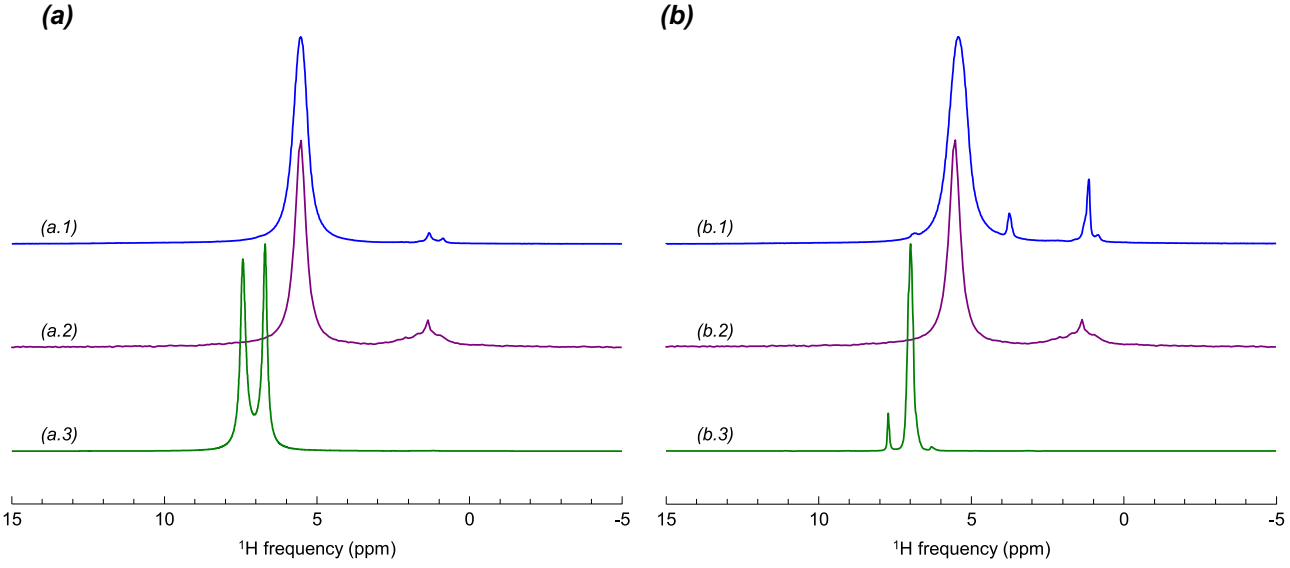

Fig. 6. ^{1}H MAS-NMR spectra of (a.1) TPA-TiO_2 and (b.1) TSA-TiO_2 along with (a.2, b.2) pristine TiO_2, (a.3) bulk TPA and (b.3) bulk TSA.

3.2. Photocatalytic activity upon UV-A and visible irradiation

Regarding the photocatalytic activity of the synthesized samples, Fig. 8 shows the photocatalytic experiments performed upon UV-A irradiation. The TPA-TiO_2 and TSA-TiO_2 samples exhibited a higher photocatalytic activity towards malachite green (MG) degradation than that of pristine sol-gel synthesized TiO_2 and Evonik P-25 powders. However, the photocatalytic activity of TPA-TiO_2 sample was slightly higher than that of TSA-TiO_2. The existence of a strong dark adsorption of MG dye on heteropolyacid-modified TiO_2 (Fig. 8a) is remarkable. This could be due to the fact that MG is a cationic dye and at pH 5.0 (pH at which experiments were performed), TPA-TiO_2 and TSA-TiO_2 samples should show a negatively charged surface since their IPs are 1.8 and 3.5, respectively, thus electrostatic interactions between the cationic dye and the modi-

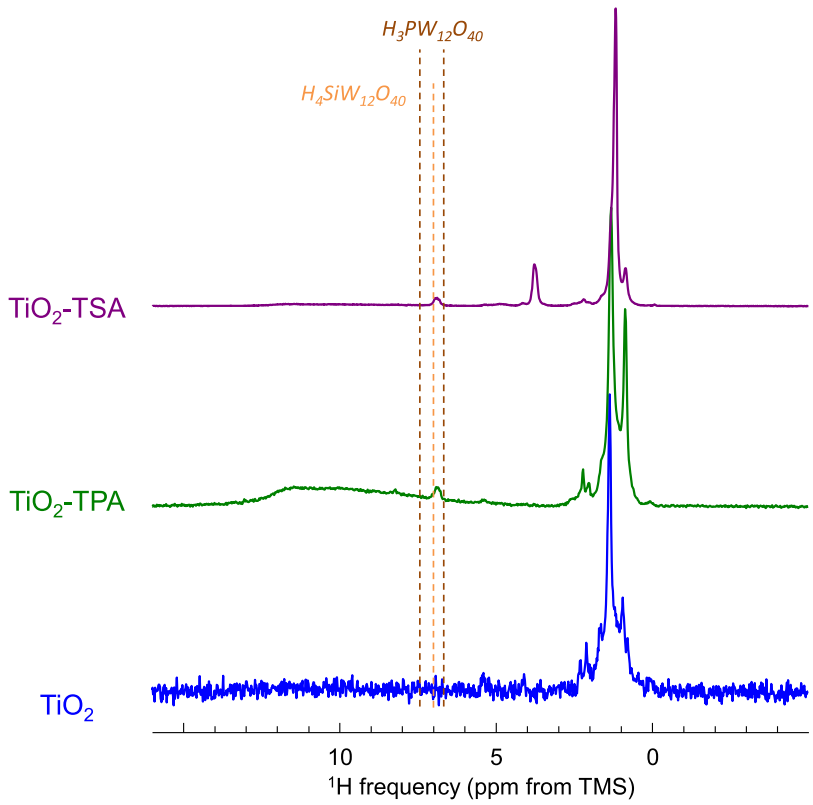

Fig. 7. ^{1}H MAS-NMR spectrum of TiO_2, TPA-TiO_2 and TSA-TiO_2 samples obtained using a long delay (5 ms) Hahn echo acquisition, selecting components with long (transverse) relaxation times.

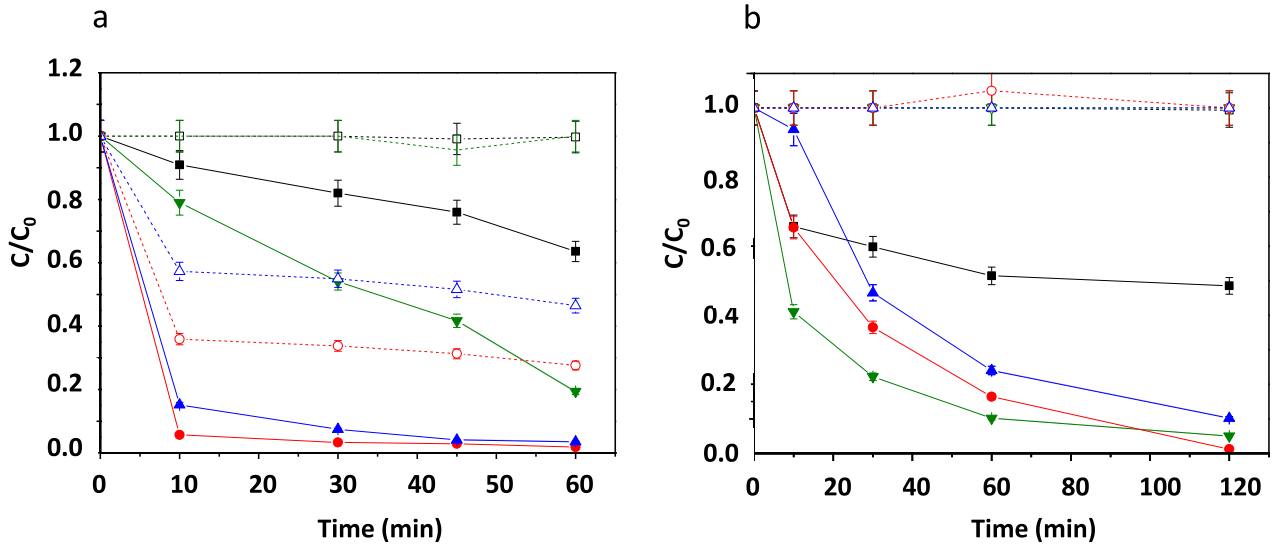

Fig. 8. Photocatalytic activity upon UV-A light irradiation of (a) malachite green and (b) 4-chlorophenol. □- dark + Pristine TiO_2; –x– MG + UV light; --△-- dark + P-25; --△-- dark+ TSA-TiO_2; --□-- dark+ TPA-TiO_2; –■– Pristine TiO_2 + UV-A; – ▼ – P-25 + UV-A; – ▲ – TSA-TiO_2 + UV-A; – ■ – TPA-TiO_2 + UV-A. (For interpretation of the references to colour in this figure legend, the reader is referred to the web version of this article.)

fied TiO_2 may take place. Results also evidenced that UV-A light did not produce malachite green degradation.

Surprisingly, 4-chlorophenol (4-CP) revealed a different behavior (Fig. 8b). In this case, Evonik P-25 showed the best photocatalytic activity upon UV-A irradiation, followed by TPA-TiO_2 and TSA-TiO_2 modified samples, respectively. In contrast, pristine sol-gel synthesized TiO_2 powder exhibited the worst performance. Dark adsorption of 4-CP was negligible.

Upon visible light irradiation, the results showed that MG was rapidly degraded by TPA-TiO_2 and TSA-TiO_2 samples (Fig. 9a); however, the former showed the highest photocatalytic activity. Evonik P-25 and pristine TiO_2 did not exhibit photocatalytic activity. On the contrary, when 4-CP was used as organic target, TPA and TSA modified TiO_2 powders showed a slight degradation (ca. 20%), while pristine TiO_2 and Evonik P-25 did not exhibit any activity (Fig. 9b).

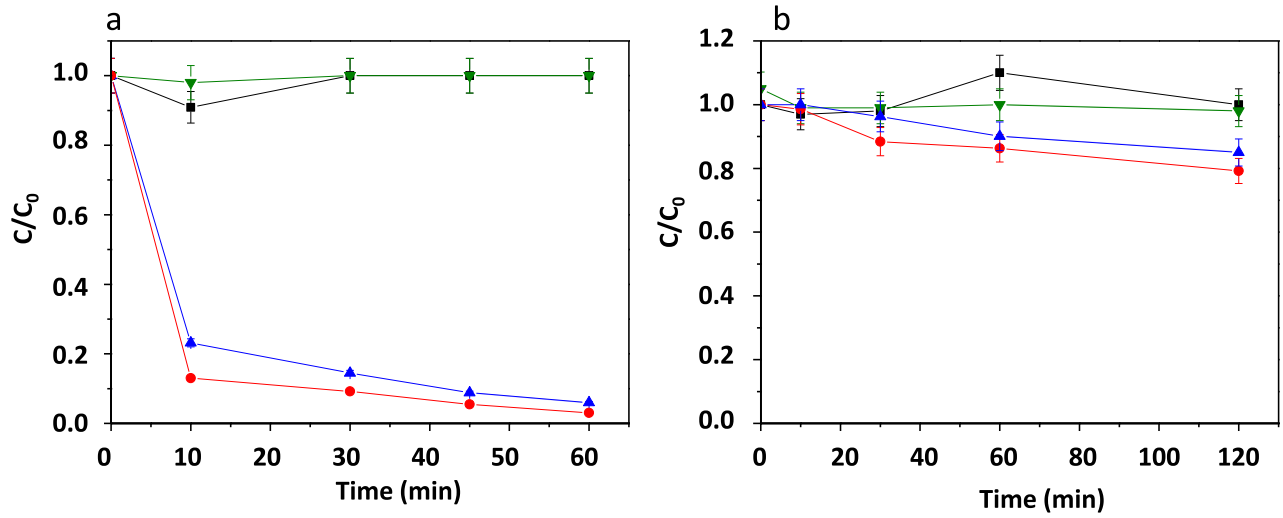

Fig. 9. Photocatalytic activity upon visible light irradiation of (a) malachite green and (b) 4-chlorophenol. -■- Pristine TiO_2 + vis; - ▼ - P-25 + vis; - ▲ - TSA-TiO_2 + vis; - ■ - TPA-TiO_2 + vis. (For interpretation of the references to colour in this figure legend, the reader is referred to the web version of this article.)

Finally, the leaching of heteropolyacids into the water from TPA-TiO_2 and TSA-TiO_2 samples was evaluated by measuring the W amount by atomic absorption spectroscopy after 4 h of UV-A irradiation. Results suggested that a small amount of the TPA or TSA initially added during the preparation of samples leached after light irradiation (0.04% for TPA-TiO_2 and 0.08% for TSA-TiO_2). This indicates high stability of the samples and that most parts of TPA and TSA are interacting strongly with the TiO_2 surface. However, further characterization studies of the modified materials after the photocatalytic process are required in order to evaluate the chemical stability of the heteropolyacids present in TiO_2.

4. Discussion

The ^{31}P and ^{29}Si MAS-NMR measurements and XPS signal of W 4f peak demonstrated that the $[PW_{12}O_{40}]^{3-}$ and $[SiW_{12}O_{40}]^{4-}$ Keggin anions should be the main species present in TiO_2 modified samples. The Keggin anion of TPA and TSA heteropolyacids is stable at low pH, thus its degradation could be neglected during the sol-gel synthesis since it was catalyzed by HCl in ethanolic media [49]. At high temperatures (T> 500 °C), a partial thermal degradation was observed in TPA-TiO_2 sample leading to the production of dimeric ($[P_2W_{21}O_{71}]^{6-}$) and lacunar ($[PW_{11}O_{39}]^{-7}$) species. On the other hand, the sol-gel synthesis involved urea addition; urea can decompose, forming ammonia (NH_4^+), which may increase the pH leading to the partial decomposition of TPA to lacunar species (Eq. 4). The latter species could lead to the production of wolframate (WO_4^{2-}), which could be the precursor of WO_x species (among them WO_3, which is a semiconductor with low band gap and visible light absorption) [49]. However, in previous studies we found that wolframate production by TPA degradation is not related to visible light absorption in TiO_2 materials modified with TPA [21].

$$[PW_{12}O_{40}]^{3-} + 6OH^- \leftrightarrow [PW_{11}O_{39}]^{7-} + [WO_4]^{2-} + 3H_2O \quad (5)$$

The ^{29}Si MAS-NMR of TSA-TiO_2 sample showed the presence of tungstosilicic or SiO_2 species. It has been previously reported that bulk TSA undergoes thermal degradation at temperatures higher than 500 °C [50], leading to the production of SiO_2 and WO_x species (Eq. 5). TSA could also be sensible to pH changes; at basic pH values, $[SiW_{12}O_{40}]^{4-}$ can be transformed to $[SiW_{11}O_{39}]^{8-}$ and $[SiW_9O_{34}]^{10-}$ lacunary isomers [51]. However, herein their presence could not be established. XRD and XPS measurements did not reveal the presence of WO_3, thus the participation of the latter in visible light absorption could be discarded.

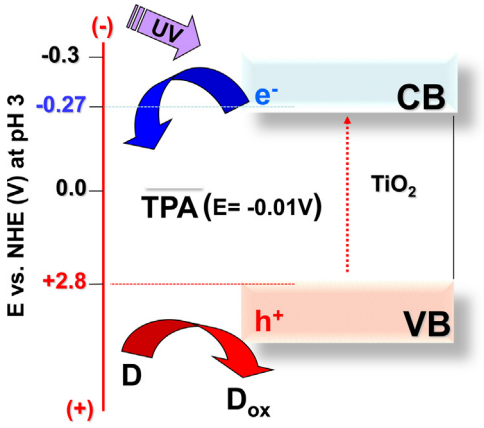

Fig. 10. Mechanism suggested for the photocatalytic activity of TPA-TiO_2 and TSA-TiO_2 samples upon UV-A light irradiation.

$$H_4[SiW_{12}O_{40}] \rightarrow SiO_2 + 12WO_{2.7-3.0} + 2H_2O \quad (6)$$

The Keggin anions of both heteropolyacids or some of their degradation by-products should be on the TiO_2 surface since SEM-EDX analysis revealed the presence of W and Si in TPA-TiO_2 and TSA-TiO_2 samples, respectively; however, since the heteropolyacids were added during the sol-gel synthesis, these species could also be present in the solid bulk.

It is highly possible that TPA ($H_3PW_{12}O_{40}$, which has three highly acid protons) protonates Ti-OH groups (formed during the sol-gel synthesis), inducing the formation of $(TiOH_2^+)(H_2PW_{12}O_{40}^-)$ and $(Ti\text{-}OH_2^+)_2(HPW_{12}O_{40}^{2-})$ species through electrostatic interactions.

However, after annealing some acid species $(TiOH_2^+)(H_2PW_{12}O_{40}^-)$ and $(Ti\text{-}OH_2^+)_2(HPW_{12}O_{40}^{2-})$ can remain anchored to the TiO_2 surface through electrostatic interactions, being responsible for the acidity found in the TPA-TiO_2 sample, as well as the low IP and the ^1H signals found at 7 ppm and the shift of the XPS O 1 s peak at 531 eV.

Something similar can be suggested for TSA-TiO_2 sample. The tungstosilicic acid ($H_4SiW_{12}O_{40}$) exhibits four protons available to interact with one, two or three Ti—OH groups by forming surface

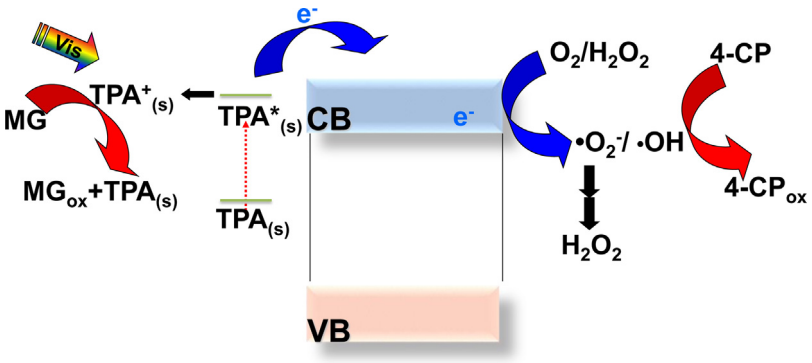

Fig. 11. Mechanism suggested for the photocatalytic activity of TPA-TiO_2 and TSA-TiO_2 samples upon visible light irradiation.

($\equiv TiOH_2^+)_x(H_{4-x}SiW_{12}O_{40}^{x-}$) acid species after the annealing at 500 °C. Similar results were found in SiO_2-TSA composites [23,24]. On the other hand, TSA could also form surface complex with TiO_2.

On the other hand, these results cannot explain why TPA-TiO_2 and TSA-TiO_2 samples show visible light absorption. As mentioned in the Introduction section, this is a capital issue that is still under debate. Herein, DRS results revealed visible light absorption in the heteropolyacid-modified TiO_2 powders, either on TPA-TiO_2 or TSA-TiO_2 samples. FT-Raman TiO_2 and TPA, TSA bands at 141 cm^{-1} and 900–1100 cm^{-1}, respectively, underwent a strong blue shift in the former and in the latter, an important broadening in the modified TiO_2 samples. This fact has already been mentioned in the literature and it is often linked to a strong interaction between TiO_2 and the heteropolyacid (specifically for TPA since there is no information about it for TSA) [16].

Thus the results presented here may curtail the responsibility for P-doping or the formation of WO_3-TiO_2 mixed oxides in the visible light absorption of TPA-TiO_2 and TSA-TiO_2 samples. We have previously reported that visible light absorption of TPA-TiO_2 or TSA-TiO_2 samples should be due to the formation of surface complexes between the Keggin anion and TiO_2 [21]. Several authors have argued that surface organic and inorganic complexes on TiO_2 may lead to visible light absorption [52–58]. Our study highlights a strong interaction between the heteropolyacids and TiO_2 surface, yielding acid sites on the samples. Legagneux et al. [59] have suggested that at high temperatures (T> 300 °C), in SiO_2 samples containing TPA, TPA species with an acidic proton $H[PW_{12}O_{40}]^{2-}$ could generate Si-O-W bonds, while Li et al. have argued that TPA could interact with titania surfaces through Ti—O—W covalent bonds formed by the interaction of W = O or W—O—W bonds with Ti-OH species [59,60]. Taking these findings into account, we suggest that at high temperatures (T = 500 °C), the acidic proton linked to TPA in $(TiOH^+_2)_2$ $(HPW_{12}O_{40}^{2-})$ species, which is highly reactive, could react with one of the protonated titanols, leading to water production and the formation of Ti-O-W bonds by generating a TPA-TiO_2 surface complex. The latter could be held responsible for visible light absorption and for the modifications observed in the Raman, XPS and MAS-NMR spectra.

The photocatalytic activity exhibited by these samples may also support this fact. Indeed, upon UV-A and visible light irradiation, TPA-TiO_2 and TSA-TiO_2 samples showed high light-induced MG degradation. At pH 5.0 (pH at which photocatalytic experiments are performed), the cationic dye can interact strongly with modified TiO_2 surfaces through electrostatic interactions since the IPs of the heteropolyacid-modified TiO_2 powders are low (1.8 for TPA-TiO_2 and 3.5 for TSA-TiO_2). UV-A irradiation induces the formation of TiO_2 e^-/h^+ pairs that can migrate to the semiconductor surface, leading to a classical photocatalytic reaction (Fig. 10). Electrons can be easily transferred from the TiO_2 conduction band (CB) (redox potential of CB electrons at pH 0 −0.1 V) to TPA or TSA Keggin anions on the surface (redox potentials are +0.218 and +0.054 V, respectively) [60,61], decreasing the e^-/h^+ recombination and leaving more valence band holes (h^+_{VB}) available to react either with pollutant molecules previously adsorbed on the photocatalyst surface or water molecules to yield •OH radicals. The different photocatalytic activities observed with MG and 4-CP upon UV-A irradiation could be explained by this. 4-CP is not adsorbed on TiO_2 surfaces, thus the attack should be achieved by the photoinduced •OH radicals near the TiO_2 surface, while in the case of MG, the molecule is closer to the surface and the oxidative attack may take place more efficiently. It is well known that in the photocatalytic reactions over TiO_2, molecules previously adsorbed on the semiconductor surface are more efficiently degraded than those whose adsorption is lower.

The photocatalytic activity upon visible irradiation unveils important findings. MG cationic dye was efficiently degraded under these conditions, while 4-CP only underwent incipient degradation. If TPA-TiO_2 or TSA-TiO_2 surface complexes are activated by visible light, an excited state of the heteropolyacid-TiO_2 complex may be induced. The excited states of HPA can directly oxidize organic compounds by electron transfer resulting in its reduction through photosensitized reactions. This oxidation is favored when the organic molecule is preassociated with the HPA [26]. Thus, the excited state of the heteropolyacid-TiO_2 complex could directly oxidize the MG molecules that are previously adsorbed at the surface, resulting in a photosensitized reaction. The reduced TPA-TiO_2 surface complex could then be reoxidized by molecular oxygen. Another photosensitized mechanism induced by visible light absorption could also take place. In this scenario, the excited state of the TPA-TiO_2 or TSA-TiO_2 complex could inject an electron into the TiO_2 conduction band. This electron could then migrate to the semiconductor surface taking place redox reactions mediated by molecular oxygen, leading to the formation of •OH radicals through the formation of superoxide radicals ($^{\bullet}O_2^-$) and its disproportion to H_2O_2 [62] (Fig. 11). Hydrogen peroxide can undergo a reduction by e^-_{CB}, producing •OH. However, the production of H_2O_2 through disproportion of superoxide radicals is extremely low in irradiated TiO_2 surfaces [63,64], which should account for the low degradation of 4-CP.

5. Conclusions

TiO_2 synthesized by the sol-gel method and subsequently modified with tungstophosphoric (TPA) and tungstosilicic (TSA) acids led to the formation of visible light absorbing nanoparticles. This fact could be induced by the generation of surface complexes between Keggin anions of HPAs and TiO_2 through the formation of Ti—O—W bonds. The characterization of the synthesized materials revealed

the presence of acid sites, probably caused by the presence of acid species of the Keggin anions.

TPA-TiO_2 and TSA-TiO_2 materials exhibited high photocatalytic activity upon UV-A irradiation, leading to a classical photocatalytic mechanism that, however, it was found to be higher for strongly adsorbed organic target. On the other hand, the high photocatalytic activity could also attributed to heteropolyacids, which have more positive redox potentials than the TiO_2 conduction band, and may induce low e^-/h^+ recombination in modified nanoparticles. Upon visible light irradiation, a different mechanism with two photosensitized paths was suggested: (i) a mechanism where the excited state of the TiO_2-HPA complex should act as an electron acceptor (from the organic substrate), oxidizing only organic molecules strongly adsorbed on the photocatalyst surface (near or on the HPA-TiO_2 surface complex sites) and (ii) a second one where the excited state of the TiO_2-HPA complex may inject an electron into the TiO_2 conduction band, inducing the formation a reduction path involving H_2O_2 production of $^{\bullet}OH$ radicals that could attack adsorbed or not adsorbed organic molecules.

Finally, TPA-TiO_2 and TSA-TiO_2 materials seem to be stable since tungsten leaching after 4 h of UV-A irradiation was very low; however, further studies about the stability of TPA and TSA present in TiO_2 after UV or visible light irradiations are necessary.

Acknowledgements

Authors thank the financial support from the Consejo Nacional de Investigaciones Científicas y Técnicas (CONICET) and Universidad Nacional de La Plata (UNLP).

Appendix A. Supplementary data

Supplementary data associated with this article can be found, in the online version, at http://dx.doi.org/10.1016/j.apcatb.2016.02.033.

References

[1] M.R. Hoffmann, S.T. Martin, W. Choi, D.W. Bahnemann, Chem. Rev. 95 (1995) 69.
[2] T. Ochiai, A. Fujishima, J. Photochem. Photobiol. C 13 (2012) 247–262.
[3] J. Chen, F. Qiu, W. Xu, S. Cao, H. Zhu, Appl. Catal. A Gen. 495 (2015) 131–140.
[4] C. Chen, W. Ma, J. Zhao, Chem. Soc. Rev. 39 (2010) 4206–4219.
[5] T. Berger, M. Sterrer, O. Diwald, E. Knozinger, D. Panayotov, T.L. Thompson, J.T. Yates, J. Phys. Chem. B 109 (2005) 6061–6068.
[6] M. Pelaez, N.T. Nolan, S.C. Pillai, M.K. Seery, P. Falaras, A.G. Kontos, P.S.M. Dunlop, J.W.J. Hamilton, J.A. Byrne, K. O'shea, M.H. Entesari, D.D. Dionysiou, Appl. Catal. B Environ. 125 (2012) 331–349.
[7] L. Gomathi-Devi, R. Kavitha, Appl. Catal. B Environ. 140–141 (2013) 559–587.
[8] R. Marschall, L. Wang, Catal. Today 225 (2014) 111–135.
[9] R. Asahi, T. Morikawa, H. Irie, T. Ohwaki, Chem. Rev. 114 (2014) 9824–9852.
[10] V.M. Zainullina, V.P. Zhukov, M.A. Korotin, J. Photochem. Photobiol. C 22 (2015) 58–83.
[11] V. Fuchs, L. Méndez, M. Blanco, L. Pizzio, Appl. Catal. A Gen. 358 (2009) 73–78.
[12] P. Ngaotrakanwiwat, S. Saitoh, Y. Ohko, T. Tatsuma, A. Fujishima, J. Electrochem. Soc. 150 (2003) A1405–A1407.
[13] T. Li, S. Gao, F. Li, R. Cao, J. Colloid Interfaces Sci. 338 (2009) 500–505.
[14] C. Yu, J.C. Yu, W. Zhou, K. Yang, Catal. Lett. 140 (2010) 172–183.
[15] S.M. Kumbar, G.V. Shanbhag, F. Lefebvre, S.B. Halligudi, J. Mol. Catal. A Chem. 256 (2006) 324–334.
[16] J. Li, W. Kang, X. Yang, X. Yu, L. Xu, Y. Guo, H. Fang, S. Zhang, Desalination 255 (2010) 107–116.
[17] N. Lu, Y. Zhao, H. Liu, Y. Guo, H. Xu, H. Peng, H. Qin, J. Hazard. Mater. 199–200 (2012) 1–8.
[18] N. Serpone, J. Phys. Chem. B 110 (2006) 24287–24293.
[19] J.A. Rengifo-Herrera, M.N. Blanco, L.R. Pizzio, Appl. Catal. B 110 (2011) 126–132.
[20] J.A. Rengifo-Herrera, R. Frenzel, M.N. Blanco, L.R. Pizzio, J. Photochem. Photobiol. A 289 (2014) 22–30.
[21] J.A. Rengifo-Herrera, M.N. Blanco, L.R. Pizzio, Mater. Res. Bull. 49 (2014) 618–624.
[22] Y. Yang, Q. Wu, C. Hu, E. Wang, J. Mol. Catal. A Chem. 225 (2005) 203–212.
[23] Y. Guo, Y. Yang, C. Hu, C. Guo, E. Wang, S. Feng, J. Mater. Chem. 12 (2002) 3046–3052.
[24] Y. Guo, C. Hu, J. Clust. Sci. 14 (2003) 505–526.
[25] J.T. Yates, Surf. Sci. 603 (2009) 1605–1612.
[26] E. Papaconstantinou, Chem. Soc. Rev. 19 (1989) 1–31.
[27] G.J. Soler-Illia, M. Jobaggy, R.J. Candal, A.E. Regazzoni, M.A. Blesa, J. Dispers. Sci. Technol. 19 (1998) 207–228.
[28] S. Gelover, P. Mondragon, A. Jimenez, J. Photochem. Photobiol. A 165 (2004) 241–246.
[29] V.M. Fuchs, E.L. Soto, M.N. Blanco, L.R. Pizzio, J. Colloid Interfaces Sci. 327 (2008) 403–411.
[30] A. Li Bassi, D. Cattaneo, V. Russo, C.E. Bottani, E. Barborini, T. Mazza, P. Piseri, P. Milani, F.O. Ernst, K. Wegner, S.E. Pratsinis, J. Appl. Phys. 98 (2005) 074305-1–074305-9.
[31] I. Holclajtner-Antunovic, D. Bajuk-Bogdanovic, A. Popa, S. Uskokovic-Markovic, Inorg. Chim. Acta 383 (2012) 26–32.
[32] M.B. Colovic, D. Bajuk-Bogdanovic, N.S. Avramovic, I. Holclajtner-Antunovic, N.S. Bosnjakovic-Pavlovic, V.M. Vasic, D.Z. Krstic, Bioorg. Med. Chem. 19 (2011) 7063–7069.
[33] D.P. Sawant, A. Vinu, S.P. Mirajkar, F. Lefebvre, K. Ariga, S. Anandan, T. Mori, C. Nishimura, S.B. Halligudi, J. Mol. Catal. A Chem. 271 (2007) 46–56.
[34] M. Pelaez, P. Falaras, V. Likadimos, A.G. Kontos, A.A. De la Cruz, K. O'shea, D. Dyonysiou, Appl. Catal. B Env. 99 (2010) 378–387.
[35] G. Colon, M.C. Hidalgo, J.A. Navio, A. Kubacka, M. Fernandez-Garcia, Appl. Catal. B Environ. 90 (2009) 633–641.
[36] J.C. Parker, R.W. Siegel, Appl. Phys. Lett. 57 (1990) 943–945.
[37] P.A. Jalil, M. Faiz, M. Tabet, N.M. Hamdan, Z. Hussain, J. Catal. 217 (2003) 292–297.
[38] R. Dziembaj, A. Malecka, Z. Piwowarska, A. Bielanski, J. Mol. Catal. A Chem. 12 (1996) 423–430.
[39] L.Q. Wang, D.R. Baer, M.H. Engelhard, Surf. Sci. 320 (1994) 295–306.
[40] L.J. Meng, C.P. Moreira de Sa, M.P. Dos Santos, Thin Solid Films. 239 (1994) 117–122.
[41] D.O. Bennardi, G.P. Romanelli, J.C. Autino, L.R. Pizzio, Appl. Catal. 324 (2007) 62–68.
[42] L.R. Pizzio, M.N. Blanco, Appl. Catal. A Gen. 255 (2003) 265–277.
[43] M.A. Henderson, Surf. Sci. Rep. 66 (2011) 185–297.
[44] F. Lefebvre, J. Chem. Soc. Chem. Commun. 10 (1992) 756–757.
[45] N. Essayem, Y.Y. Tong, H. Jobic, J.C. Vedrine, Appl. Catal. A Gen. 194–195 (2000) 109–122.
[46] J.C. Edwards, C.Y. Thiel, B. Benac, J.F. Knifton, Catal. Lett. 51 (1998) 77–83.
[47] V. Brahmkhatri, A. Patel, Ind. Eng. Chem. Res. 50 (2011) 13693–13702.
[48] M. Crocker, A.M. Herold, A.E. Wilson, M. Mackay, C.A. Emeis, A.M. Hoogendoorn, J. Chem. Soc. Faraday Trans. 92 (1996) 2791–2798.
[49] M.T. Pope, Heteropoly and Isopolyoxometalates, Springer-Verlag, Heidelberg, 1983, pp. p58.
[50] M. Klisch, J. Sol-gel Sci. Technol. 12 (1998) 21–33.
[51] A. Tézé, G. Hervé, J. Inorg. Nucl. Chem. 39 (1977) 999–1002.
[52] G. Kim, W. Choi, Appl. Catal. B Environ. 100 (2010) 77–83.
[53] S. Kim, W. Choi, J. Phys. Chem. B 109 (2005) 5143–5149.
[54] C. Chen, W. Ma, J. Zhao, Chem. Soc. Rev. 39 (2010) 4206–4219.
[55] M. Li, Z. Hong, Y. Fang, F. Huang, Mater. Res. Bull. 43 (2008) 2179–2186.
[56] G. Zhang, G. Kim, W. Choi, Energy Environ. Sci. 7 (2014) 954–966.
[57] K. Li, Y. Guo, F. Ma, H. Li, L. Chen, Y. Guo, Catal. Commun. 11 (2010) 839–843.
[58] K. Li, X. Yang, Y. Guo, F. Ma, H. Li, L. Chen, Y. Guo, Appl. Catal. B Environ. 99 (2010) 364–375.
[59] N. Legagneux, J.M. Basset, A. Thomas, F. Lefebvre, A. Goguet, J. Sa, C. Hardacre, Dalton Trans. 12 (2009) 2235–2240.
[60] A. Nakajima, T. Koike, S. Yanagida, T. Isobe, Y. Kameshima, K. Okada, Appl. Catal. A Gen. 385 (2010) 130–135.
[61] K. Pruethiarenun, T. Isobe, S. Matsushita, J. Ye, A. Nakajima, Mater. Chem. Phys. 144 (2014) 327–334.
[62] D.T. Sawyer, Acc. Chem. Res. 14 (1981) 393–400.
[63] Y. Nosaka, Y. Yamashita, H. Fukuyama, J. Phys. Chem. B 101 (1997) 5822–5827.
[64] H. Sakai, R. Baba, K. Hashimoto, A. Fujishima, A. Heller, J. Phys. Chem. B 99 (1995) 11896–11900.